Understanding the Complexation of Eu^{3+} with Diglycolamide-Functionalized Calix[4]arenes: Spectroscopic and DFT Studies†

Seraj Ahmed Ansari,[a] Prasanta Kumar Mohapatra,[a,*] Sheikh Musharaf Ali,[b] Arijit Sengupta,[a] Arunasis Bhattacharyya,[a] and Willem Verboom[c]

[a]*Radiochemistry Division, Bhabha Atomic Research Centre, Trombay, Mumbai-400085, India*

[b]*Chemical Engineering Division, Bhabha Atomic Research Centre, Trombay, Mumbai-400085, India*

[c]*Laboratory of Molecular Nanofabrication, MESA+ Institute for Nanotechnology, University of Twente, P.O. Box 217, 7500 AE Enschede, The Netherlands*

ELECTRONIC SUPPORTING INFORMATION

Contents

1. Experimental

1.1 Materials.

Narrow rim DGA-functionalized calix[4]arene (**L_I**) was synthesized by reaction of cone tetrakis-(aminopropoxy)calix[4]arene with *p*-nitrophenol activated diglycolamide. The wide rim (**L_{II}**) and bothrims (**L_{III}**) DGA-functionalized calix[4]arenes (Figure 1 of main text) were prepared accordingly by reaction of the known tetrabutoxycalix[4]arene tetraamine and octaaminocalix[4]arene with *p*-nitrophenol-activated diglycolamide, respectively. The detailed synthesis procedure has been described elsewhere.[1] The ligands were characterized by elemental analysis, ^{1}H-NMR, IR spectroscopy, as well as by mass spectrometry. Acetonitrile (99.8%) was procured from Sigma Aldrich and was used as received. Stock solutions of Eu^{3+} ions were prepared by dissolving $Eu(NO_3)_3$ salt, procured from Sigma-Aldrich with a purity of 99.9%, in acetonitrile and its concentration in the stock was confirmed by EDTA complexometric titration using methyl thymol blue as the indicator. All the other reagents were of AR grade and were used without further purification.

1.2 Spectrophotometry.

UV-Vis absorption spectra of the ligands in acetonitrile were collected in the wavelength region 190-320 nm (0.1 nm interval) on a double beam Jasco V-530 spectrophotometer using a 10 mm path length quartz cell. Complexometric titrations were done by following the ligand spectra after addition of each increment of the $Eu(NO_3)_3$ solution. In each titration, appropriate aliquots of the titrant (Eu^{3+}) were added into the cell and mixed thoroughly for about 2 minutes before the spectrum was recorded. The mixing time was found to be sufficient to complete the complexation reaction. Usually, 15-20 spectra were recorded in each set of titration.

1.3 NMR spectral analysis.

The NMR spectral studies were carried out using free ligand sample in CD_4OD for which ^{1}H and ^{13}C spectra were recorded. To the sample, a slight excess of the

calculated amount of La(III) triflate (for 1:1 complex) was added and the samples were recorded again. A Varian 500 MHz machine was used for the NMR studies.

1.4 Microcalorimetry.

Calorimetric titrations were performed with an isothermal titration microcalorimeter (TAMIII), which measures the heat flow between the reaction vessel, reference vessel, and a heat sink maintained at a constant temperature. The gain factors were calibrated by the instrument before each experiment. The system was allowed to equilibrate for sufficient time before making a baseline measurement. The reaction cup initially contained 2.7 mL of the titrant which was stirred with a basket rotor maintained at 80 rpm. The injections of titrant were made through a Hamilton 500 µL syringe. When the system reached thermal equilibrium, 25 µL of titrant were injected into the reaction vessel and the heat flow was recorded. About 20 titration data were obtained for each experiment.

1.5 Emission Spectroscopy.

Luminescence studies were performed with an Edinburgh F-900 Fluorescence Spectrometer equipped with a xenon lamp as excitation source, M-300 monochromators, and a Peltier cooled photo multiplier tube as detector. The luminescence emission spectra were obtained in the wavelength region of 550–750 nm (1.0 nm/step) by excitation at 395 nm (5 nm bandwidth). Similarly, the luminescence lifetime data were recorded at an excitation wavelength of 395±5 nm and the decay curve was followed at an emission wavelength of 612±5 nm. The acquisition and analysis of the data were carried out by F-900 software supplied by Edinburgh Analytical Instruments, UK.

1.6 Computational Studies.

Structures of the free ligands ($\mathbf{L_I}$, $\mathbf{L_{II}}$, and $\mathbf{L_{III}}$) and their complexes with Eu^{3+} cation in presence of a nitrate ion were optimized using the Becke-Lee-Young-Parr (B3LYP) density functional[2] employing the split-valence plus polarization (SVP) basis set,[3] as implemented in the TURBOMOLE suite of program.[4] The scalar relativistic effective

core potentials (ECP) were used for the Eu^{3+} ion with 28 core electrons.[5] The septate spin state was used during the computation and optimization was performed without any symmetry restrictions. The solvent phase was accounted for using the popular conductor like screening model (COSMO),[5(d)] where the dielectric constant of the solvent (acetonitrile) was taken as 37.5. The following complexation reaction model in the acetonitrile medium was used in the computation:

$$Eu^{3+}(H_2O)_9 + 3NO_3^- + L \quad <===> \quad Eu(NO_3)_3{\cdot}L + 9\,H_2O \qquad (1)$$

Here, the stoichiometry of the complex was taken as 1:1 from the literature.[6] Scalar relativistic effects for heavier lanthanide and actinide elements were included in the present computation as described earlier.[7] Since there is a very small effect on the solvation energy between the gas phase and the solvent phase geometry,[8] the aqueous solvent effect was integrated by performing single point energy calculations using the optimized geometry obtained from the B3LYP level of theory employing the COSMO solvation model.

2. Results & Discussion

2.1 UV-Vis spectrophotometry

The stability constants of the Eu^{3+}/L complexes were calculated by nonlinear least-squares regression analysis using the Hyperquad suit program,[9] based on equilibrium reaction (1).

$$Eu^{3+} + iL <===> Eu(L_i)^{3+} \qquad (2)$$

$$\beta_i = [Eu(L_i)^{3+}] / [Eu^{3+}]\,[L]^i \qquad (3)$$

where, β_i is the overall complex formation constant of the i'th complex.

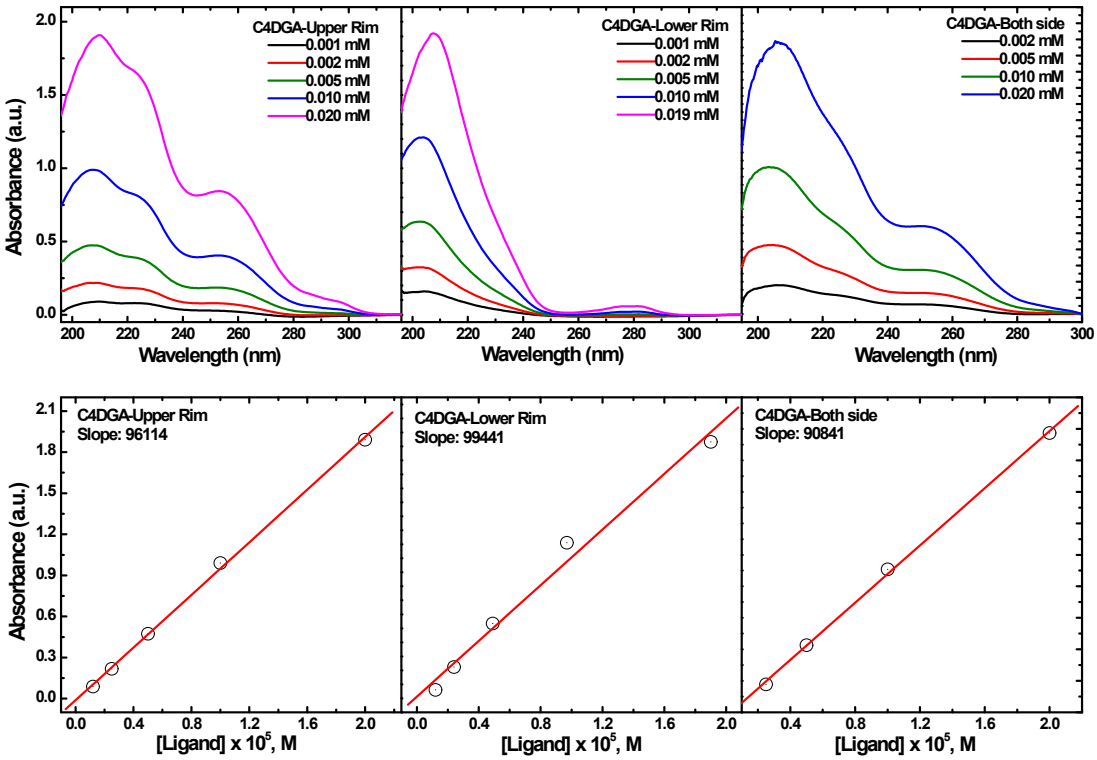

Figure S1. Absorption spectra of C4DGA ligands $\mathbf{L_I}$, $\mathbf{L_{II}}$, and $\mathbf{L_{III}}$ in BumimTf_2N, and Beer's plot; Ligand concentration: 0.001 – 0.02 mmol/L; Temperature: 25 °C.

2.2 NMR spectral analysis

The ^{1}H and ^{13}C NMR spectra of the free ligand $\mathbf{L_I}$ and its La(III) triflate complex are presented below.

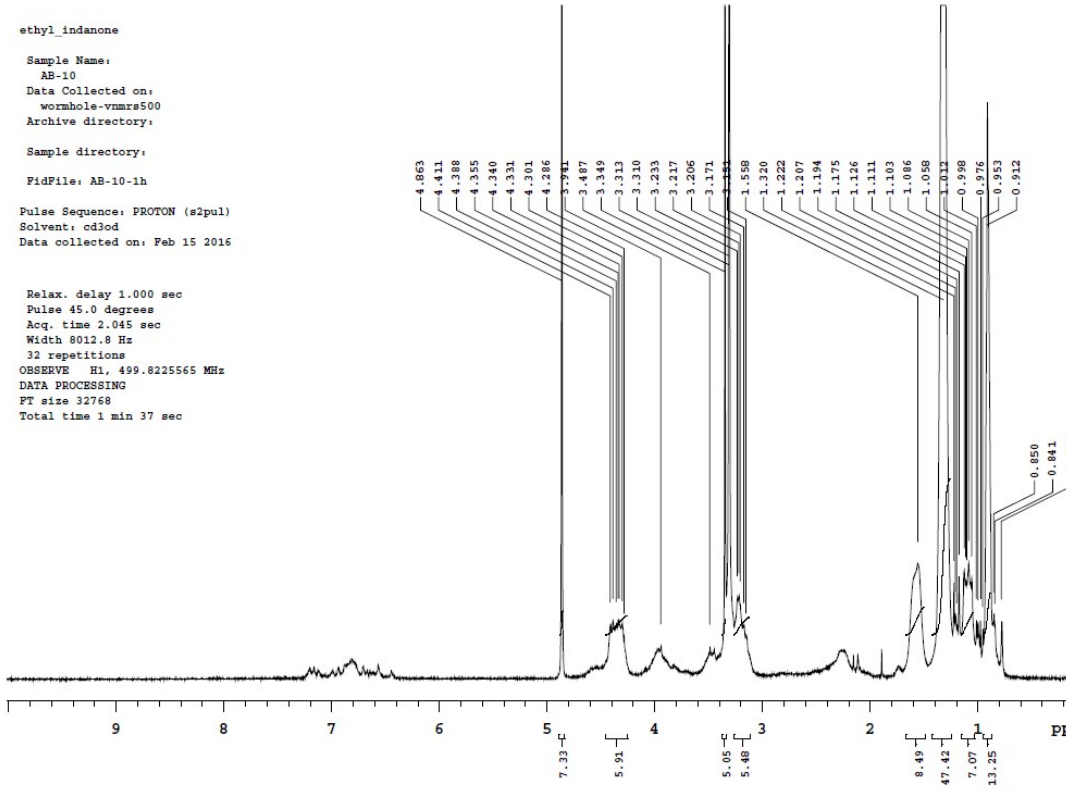

Figure S2. ^{1}H NMR spectrum of $\mathbf{L_I}$ in CD_3OD.

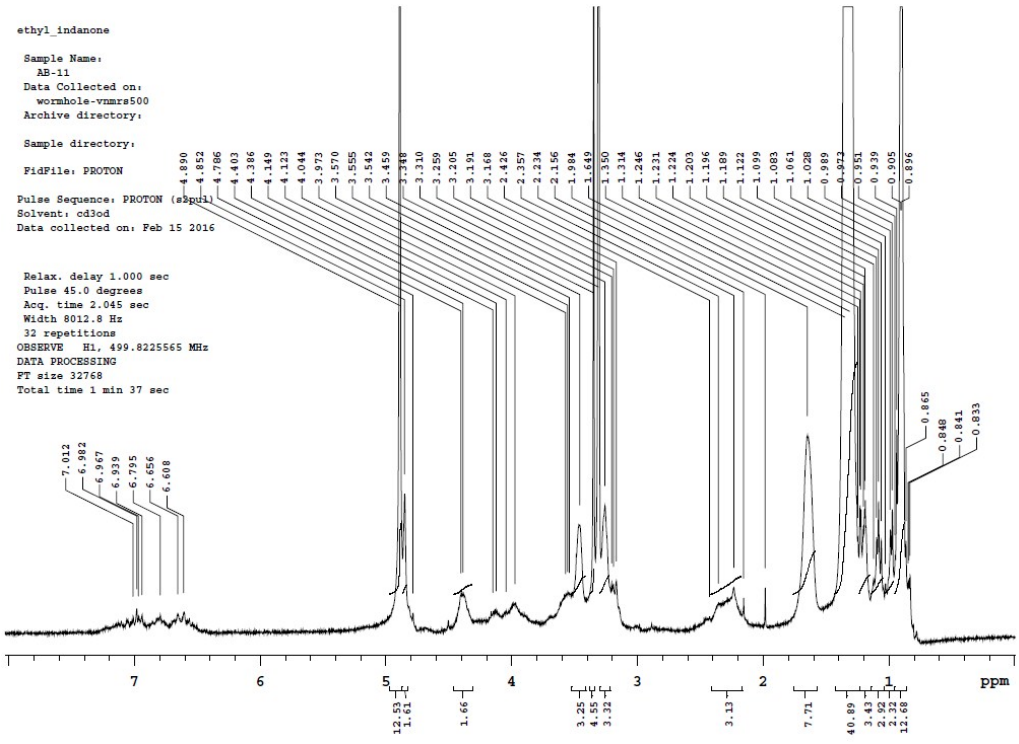

Figure S3. ^{1}H NMR spectrum of $\mathbf{L_I}$ + La(III)-triflate in CD_3OD.

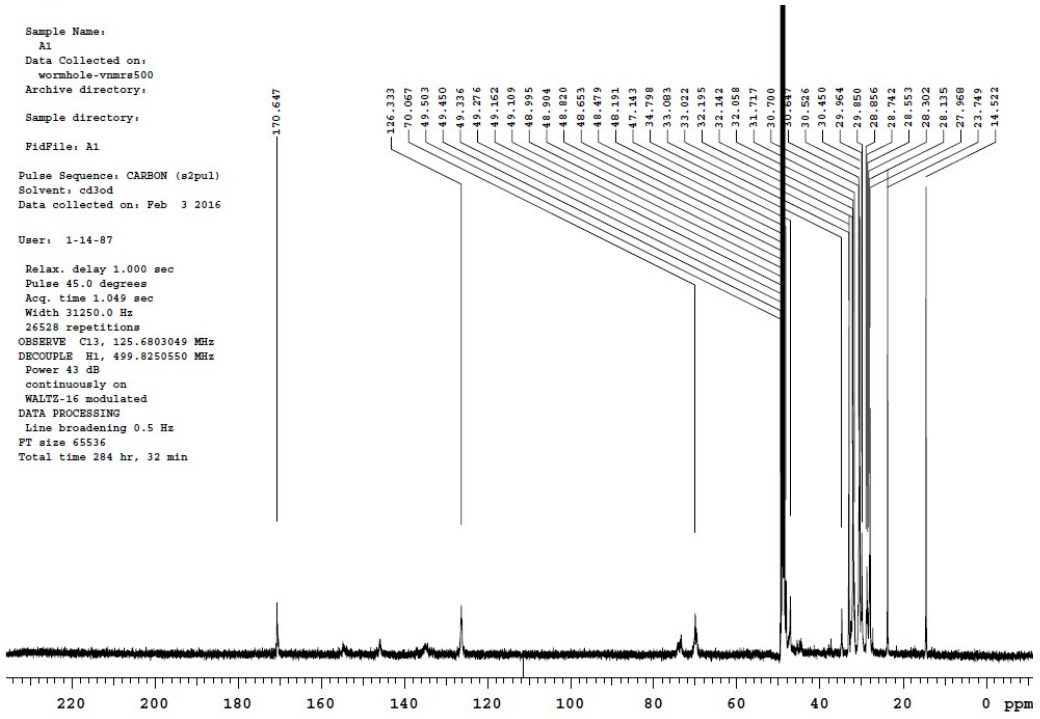

Figure S4. ^{13}C NMR spectrum of $\mathbf{L_I}$ in CD_3OD.

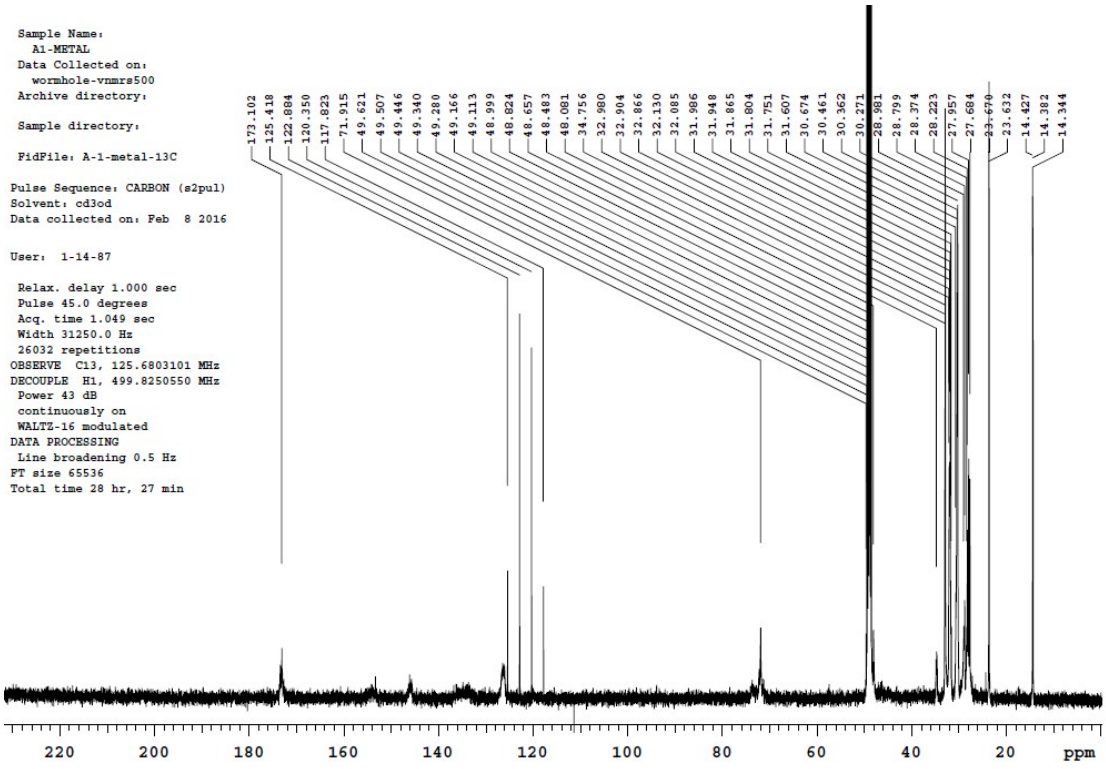

Figure S5. ^{13}C NMR spectrum of $\mathbf{L_I}$ + La(III)-triflate in CD_3OD.

2.3 Microcalorimetry

The heat obtained at each titration point was fitted in HypdelH program,[9] in conjunction with stability constant data, to get enthalpy of reaction.

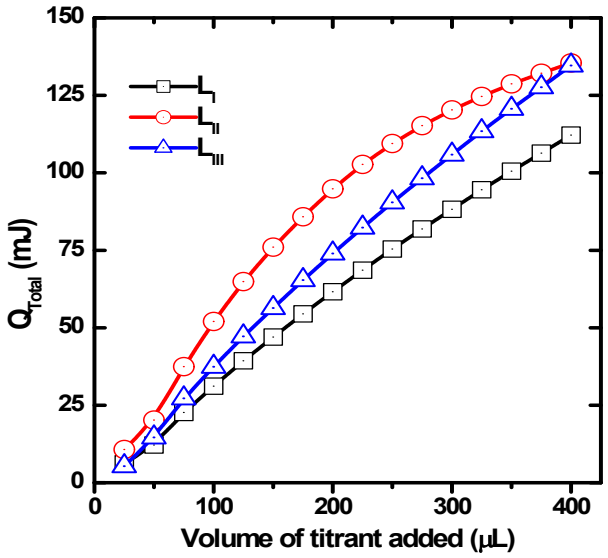

Figure S6. Cumulative heat of titration of $Eu(NO)_3$ with $\mathbf{L_I}$, $\mathbf{L_{II}}$ and $\mathbf{L_{III}}$ as a function of the titrant volume. Open symbols: experimental heat, solid lines: fitted heat.

2.4 ESI-MS of the complexes

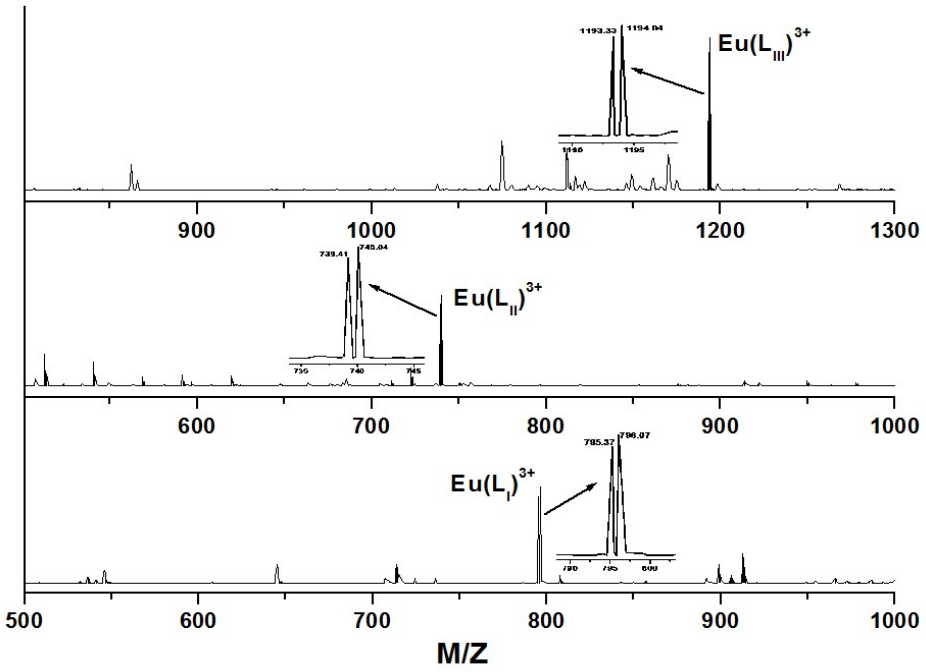

Figure S7. ESI-MS spectra confirming the presence of $Eu(L)^{3+}$ complexes without nitrate and water molecules. The insets indicate the isotopic composition due to Eu-151 and Eu-153.

2.5 Emission spectroscopy

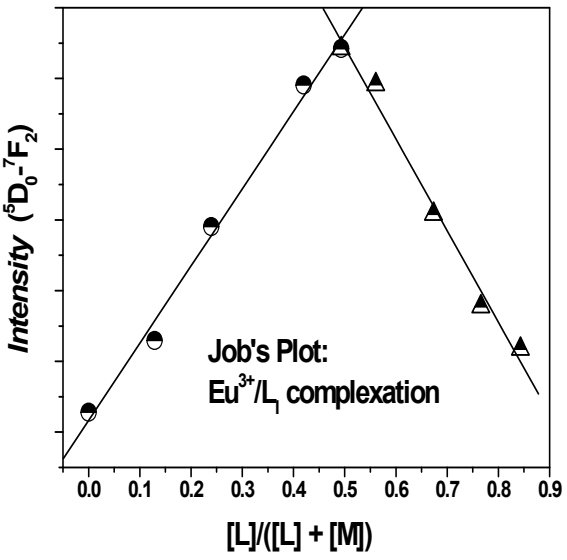

Figure S8. Job's plot for determination of the stoichiometry of the Eu^{3+}/**L_I** complex.

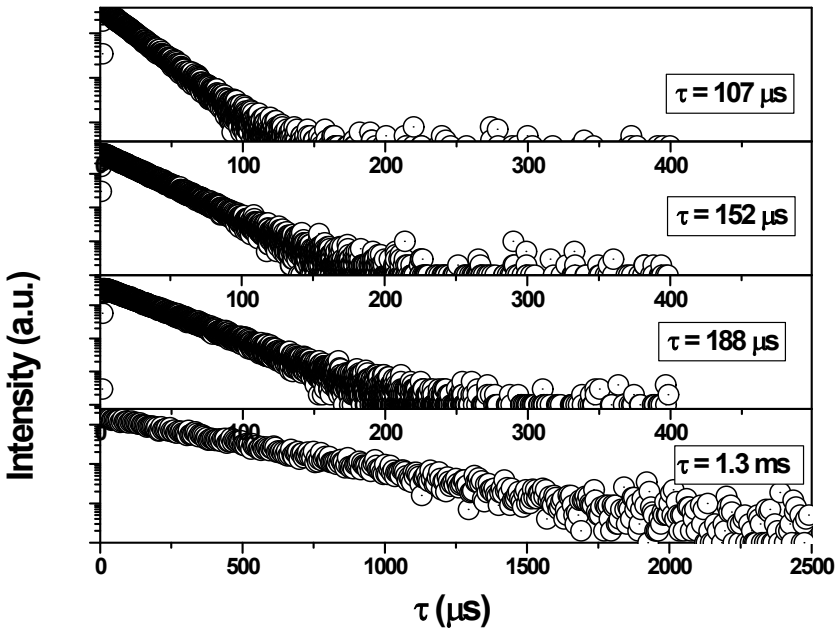

Figure S9. Luminescence decay curve of $Eu^{3+}/\mathbf{L_I}$ complexation. Excitation wavelength: 395 ± 5 nm; Emission wavelength: 615 ± 5 nm. Cuvette solution: 1.0 mmol/L $Eu(NO_3)_3$ containing varying concentration of $\mathbf{L_I}$; Temperature: 25 °C.

Table S1. Luminescence lifetime of the $Eu^{3+}/\mathbf{L_I}$ complex and the calculated number of water molecules (N_{H2O}) in the primary coordination sphere. $[Eu^{3+}]_{total}$ = 1 mmol/L. Experimental conditions are identical to those in Figure 3.

C_L / C_{Eu}	τ (ms)	$N_{H2O\ (expt)}$	% $[Eu^{3+}]$ free	*% [Eu·L] complex*	$N_{H2O\ (Cal)}$[a]	$N_{H2O\ (Cal)}$[b]
0	0.107	9.1	100	0	9.0	9.0
0.08	0.111	8.8	84.46	15.54	8.1	7.6
0.16	0.128	7.5	71.51	28.49	7.3	6.4
0.33	0.152	6.2	48.2	51.8	5.9	4.3
0.49	0.188	4.9	29.21	70.79	4.8	2.6
0.82	0.750	0.7	0.19	99.81	3.0	0.0
0.98	1.31	0.1	0.04	99.96	3.0	0.0
1.3	1.31	0.1	0.02	99.98	3.0	0.0
1.5	1.31	0.1	0.02	99.98	3.0	0.0

[a]*Assuming two-arm coordination.* [b]*Assuming three-arm coordination.*

2.6 Computational studies

2.5.1 Structural parameters

The minimum energy structures of free C4DGA ($\mathbf{L_I}$) and its complexes with Eu^{3+} are displayed in **Fig. S6.** In **Fig. S6**, the four DGA group was shown to be linked to the four phenolic OH of calix[4]arene moiety in little asymmetric manner. The structural parameters for the nitrate complexes of Eu3+ with both the ligands are presented in Table S2.

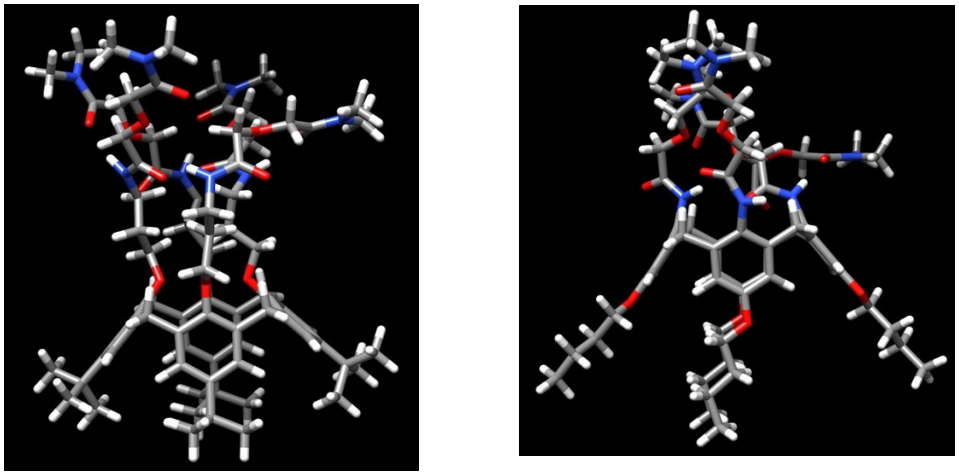

Figure S10: Minimum energy structure of free L_I (left) and L_{II} (right) at BP/SVP level of theory

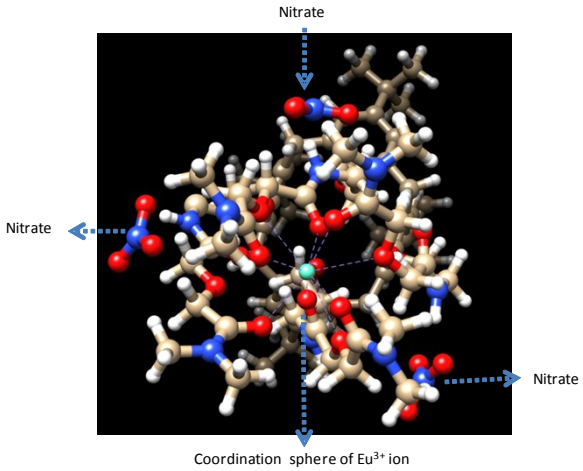

Figure S11: Full view of coordinating sphere of Eu^{3+} ion with L_I and nitrate ions (L_I).

Table S2. Calculated structural parameters in Å at the B3LYP level of theory using the SVP basis set

Complex	Eu-O (Å) (>C=O)	Eu-O (Å) (Ether)	Eu-C (Å) (>C=O)	Eu-C (Å) (Ether)	Eu-N(Å) (NO_3)
$\mathbf{L_I}$/Eu$(NO_3)_3$	2.443	2.762	3.430	3.990	5.77
	2.418	2.737	3.390	3.63	5.73
	2.389	2.704	3.390	3.61	5.97
	2.406	3.520	3.35	3.615	
	2.380		3.33		
	2.468		3.344		
	4.390		4.72		
	5.025		4.83		
$\mathbf{L_{II}}$/Eu$(NO_3)_3$	2.434	2.537	3.304	3.522	5.747
	2.391	2.737	3.246	3.696	5.108
	2.649	2.538	3.447	3.448	4.923
	2.482	4.430	3.523	4.658	
	2.371		3.239		
	2.568		3.854		
	3.701		3.686		
	5.116		5.381		

2.5.2 The free energy of complexation

The free energy values for the complexation of Eu^{3+} ion with $\mathbf{L_I}$ and $\mathbf{L_{II}}$ in gas phase is presented in Table S3. The explicit hydration of the Eu^{3+} ion with 9 water molecules in the first solvation shell was considered for evaluating the complexation free energy as it was found to reproduce the experimental solvation energy quite accurately.[10] Since, most of the nuclear waste is reprocessed from aqueous environment; it will be more practical if the free energy is calculated in the solvent phase. The well known COSMO solvation approach was used to simulate the solvent

phase as it was able to predict the solvent phase properties quite accurately as demonstrated by many researchers earlier.[11]

Table S3. Calculated free energy for the complexation of Eu^{3+} with L_I and L_{II} (kcal/mol) at B3LYP level of theory using the TZVP basis set for the ligands

System	Gas phase		Acetonitrile phase	
	Binding energy	Free energy	Binding energy	Free energy
$Eu(NO_3)_3$/**L_I**	-495.80	-535.19	-8.44	-47.54
$Eu(NO_3)_3$/**L_{II}**	-469.76	-520.29	11.68	-38.85
ΔE (**L_I – L_{II}**)	-26.04	-14.90	-20.12	-8.69

2.5.3 Natural Population analysis

In order to get an insight into the nature of bonding in the complexes of metal ions with **L_I** and **L_{II}** charge on the metal ions and atomic orbital population in the complexes was analyzed using the method of natural population analysis (NPA) [ref].

Table S4: Calculated charge and orbital population using NBO analysis in gas phase at B3LYP/SVP level of theory.

System	charge	s	p	d	f	g
L_I	1.821	4.188	12.001	10.885	6.103	0.0004
L_{II}	1.783	4.178	12.003	10.855	6.178	0.0004

2.5.4 HOMO – LUMO of the complexes

Table S5. Calculated quantum chemical descriptors in the gas phase at the B3LYP/SVP level of theory

System	$\Delta E_{LUMO-HOMO}$(eV)	H	X	ΔN
$Eu^{3+}(H_2O)_9$	3.64	1.82	18.3	
L_I	3.74	2.43	1.87	2.14
L_{II}	4.77	2.78	2.39	1.84

References:

1. M. Iqbal, P. K. Mohapatra, S. A. Ansari, J. Huskens and W. Verboom, *Tetrahedron,* 2012, **68**, 7840-7847.
2. (a) A. D. Becke, *J. Chem. Phys*., 1993, **98**, 5648-5652; (b) C. Lee, W. Wang and R. G. Parr, *Phys. Rev. B,* 1988, **37**, 785-789.
3. A. Schaefer, H. Horn and R. J. Ahlrichs, *J. Chem. Phys*., 1992, **97**, 2751–2777.
4. (a) R. Ahlrichs, M. Bar, M. Haser, H. Horn and C. Kolmel, *Chem. Phys. Lett*., 1989, **162**, 165-169; (b) TURBOMOLE V6.0 2009, a development of University of Karlsruhe and Forschungszentrum Karlsruhe GmbH, 1989-2007, TURBOMOLE GmbH.
5. (a) M. Dolg, H. Stoll and H. Preuss, *J. Chem. Phys*., 1989, **90**, 1730-1734; (b) W. Kuchle, M. Dolg, H. Stoll and H. Preuss, *J. Chem. Phys*., 1994, **100**, 7535-7542; (c) X. Cao and M. Dolg, *J. Mol. Struc.-THEOCHEM,* 2004, **673**, 203-209; (d) G. A. Shamov, G. Schreckenbach and T. N. Vo, *Chem. Eur. J*., 2007, **13**, 4932-4947.
6. P. K. Mohapatra, D. R. Raut, M. Iqbal, J. Huskens and W. Verboom, *J. Membr. Sci.,* 2013, **444**, 268-275.
7. (a) C. Z. Wang, J. H. Lan, Q. Y. Wu, Y. L. Zhao, X. K. Wang, Z. F. Chai and W. Q. Shi, *Dalton Trans*., 2014, **43**, 8713-8720; (b) J. P. Justin, M. Sundararajan, M. A. Vincent, I. H. Hiller, *Dalton Trans*., 2009, **30**, 5902-5909; (c) D. Manna and T. K. Ghanty, *Phys. Chem. Chem. Phys.,* 2012, **14**, 11060-11069.
8. (a) G. A. Shamov and G. Schreckenbach, *J. Phys. Chem. A*., 2005, **109**, 10961-10974; (b) A. Boda, J. M. Joshi, Sk. M. Ali, K. T. Shenoy and S. K. Ghosh, *J. Mol. Mod.,* 2012, **19**, 5277-5291; (c) A. Boda, Sk. M. Ali, K. T. Shenoy and S. K. Ghosh, *Sep. Sci. Technol*., 2013, **48**, 2397-2409.
9. P. Gans, A. Sabatini and A.Vacca, *Talanta,* 1996, **43**, 1739-1753.
10. A. K. Singha Deb, Sk. M. Ali, K. T. Senoy and S. K. Ghosh, *Mol. Sim.*, 2015, **41**, 490-503.
11. (a) G. Schreckenbach and G. A. Shamov, *Acc. Chem. Res.*, 2010, **43**, 19-29; (b) V. S. Bryantsev and B. P. Hay, *Dalton Trans.*, 2015, **44**, 7935–7942; (c) C.-Z.

Wang, J.-H. Lan, Q.-Y. Wu, Y.-L. Zhao, X.-K. Wang, Z.-F. Chai and W.-Q. Shi, *Dalton Trans.*, 2014, **43**, 8713–8720; (d) J. Zhang, N. Heinz and M. Dolg, *Inorg. Chem.*, 2014, **53**, 7700−7708.